

Calorimetric and thermodynamic analysis of an enantioselective carboxylesterase from *Bacillus coagulans*: insights for an industrial scale-up

Francesca Saitta, Pietro Cannazza, Silvia Donzella, Valerio De Vitis, Marco Signorelli, Diego Romano, Francesco Molinari and Dimitrios Fessas*

DeFENS, Università degli Studi di Milano, Via Celoria 2, 20133 Milano, Italy

Corresponding Author: Prof. Dimitrios Fessas, DeFENS, Università di Milano, Via Celoria 2, 20133 Milano, Italy, e-mail: dimitrios.fessas@unimi.it, tel. +390250319219.

Abstract

Microbial carboxylesterases are valuable biocatalysts that can selectively hydrolyze a wide spectrum of esters and may find their own applicability at industrial scale. In this work, we report the calorimetric study of an atypical enantioselective carboxylesterase from *Bacillus coagulans* (BCE). The influence of different pH conditions (from pH 6 to 9) on BCE thermal stability was investigated through Differential Scanning Calorimetry (DSC). A complete thermodynamic analysis of the system in combination with specific activity measurements was performed for the assessment of the best working conditions for such an enzyme.

The overall results indicate that the kinetic benefits deriving from the temperature rise overwhelm the thermodynamic disadvantages in terms of protein stability, being aware that the working temperature should always be kept well below the onset of the denaturation process, which may trigger aggregation effects.

Although the results concern this specific enzyme, the methodological approach has a general validity and may be useful as a guideline to design enzyme optimal working conditions through calorimetric methods.

Keywords: Carboxylesterases; *Bacillus coagulans*; pH influence; Thermodynamic analysis; Differential Scanning Calorimetry.

1 **Introduction**

2 Carboxylesterases or carboxylester hydrolases (EC 3.1.1.1) are cofactor independent serine
3 hydrolases enzymes, able to catalyze the hydrolysis or the synthesis of carboxyl ester bonds. Usually,
4 esterases are distinguished from lipases (E.C. 3.1.1.3) based on the preferred hydrolyzed substrates:
5 esterases generally work on water-soluble substrates, while lipases act on long chain esters.
6 Considering the above-mentioned reasons, they are usually also referred respectively as non-lipolytic
7 esterases and lipolytic esterase hydrolases [1]. In the case of the hydrolysis of triglycerides, 10 carbon
8 atoms are conventionally considered as the threshold to distinguish esterase and lipases. Other
9 classifications based on interfacial activation, electrostatic distribution of protein surface, primary
10 sequence and structural features have been proposed, but none of them was found to be completely
11 effective [2,3] .

12 In all carboxylesterases, the enzymatic hydrolysis takes place in the highly conserved active site
13 among these proteins, composed by the so-called catalytic triad usually composed of an aspartate, a
14 histidine and a serine residue. Under physiological conditions, catalytic serine is activated with the
15 seizing of a proton by aspartate and histidine, then the catalytic mechanism is initiated by the
16 nucleophilic attack of the activated serine on the substrate's carbonyl. As a consequence, a tetrahedral
17 transient intermediate is formed and stabilized by two hydrogen bonds of the amide protons of the
18 oxyanion hole. Then, the hydrolyzed alcohol leaves the catalytic site while enzyme deacylation is
19 operated in the following step by the nucleophilic attack of a water molecule [4].

20 In addition to the catalytic triad and to the amino acid constituting the oxyanion hole, a common
21 structure called " α/β hydrolase fold" is highly conserved in the esterases tridimensional structures.
22 The core structure of the hydrolase fold is characterized by eight parallel strands (beside beta β -2
23 sheet) connected by alpha helices (Figure 1). Catalytic residues are usually placed along the amino
24 acid sequence, and they find place, shaping the catalytic site, only in the native protein folding.
25 Aspartate and serine are usually located respectively after β -7 and β -5 sheets, while serine is located
26 before the last α -helix, close to the C-terminal end of the protein [5].

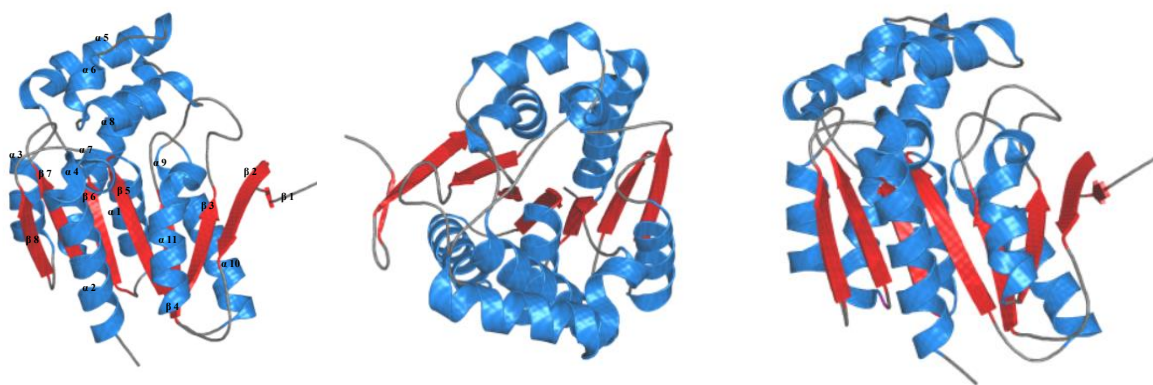


Figure 1. The crystal structure of BCE (PDB: 3JWE) at different angulations, α -Helices are represented in blue and β -strands in red colour.

Since 1973, when Eijkman isolated the first esterase from *Serratia marcescens* [6], extensive efforts have been spent by researchers in the isolation and characterization of novel esterases with variable chemo-, regio-, and enantioselectivity [7]. Due to their catalytic capabilities together with their high stability, esterases are widely employed in industrial applications in food, pharmaceutical, and oleochemical industries. Some of the worth mentioning applications of esterases include the formulation of laundry detergents, flavours development for food additives, reduction of environmental pollution, employment in the pulp and paper industry, biosensors in medical field, and as active ingredient in pharmaceuticals [8–10]. Moreover, esterases are attractive stereoselective biocatalysts [11], but their potential is still far from being fully exploited, although examples of industrial applications are known, for instance the production of (S)-naproxen [12].

For this work, among the different options, from highly active [13], organic solvent [14] and heavy metals [15] resistant, thermostable [9] and halotolerant [16] esterases, we selected to investigate a carboxylesterase from *Bacillus coagulans* (BCE) previously isolated and characterized from a biochemical and structural point of view for its industrial appealing peculiarity to enantioselectively hydrolyze different esters of the chiral alcohol 1,2-O-isopropylideneglycerol (IPG) [17,18], whose enantiomers are valuable chiral building blocks for the synthesis of β -blockers, prostaglandins and glycerophospholipids [19]. This enzyme shows an atypical behavior with a nonlipase-like activity, yet possessing a lipase-like 3D fold [18].

Considering that an enzyme's functionality and efficiency rely on both thermodynamic and kinetic factors [20–22], specific attention should be paid for the assessment of the optimal working conditions to maximize the performances of any lab-scale or industrial process.

In this context, BCE thermal stability was here studied by Differential Scanning Calorimetry (DSC) in different buffers to assess the influence of pH conditions, ranging from pH 6.0 to 9.0. The thermodynamic exploitation of these data permitted to obtain the $\Delta G^\circ(T)$ function, that is correlated with the protein functionality as concerns the thermodynamic standpoint, and the association with measurements of enzymatic specific activity allowed to dissect the functionality of BCE in view of an industrial process design. The straightforward analysis of thermostability of BCE may be extended and proposed as a methodological approach to investigate thermodynamic and kinetic aspects of an enzymatic biocatalyst for specific industrial applications.

Materials and Methods

Protein expression and purification

The protein was expressed and purified following De Vitis *et al.* protocol with some slight modifications [18]. For protein expression, pET100 plasmid carrying BCE gene fused with a N-terminal his-tag (accession number WP_029142894) was transformed into chemically competent *E. coli* BL21 (DE3). Single colonies from LB-agar plates supplemented with 100 mg/L of ampicillin, grown overnight at 37°C, were inoculated into 20 mL of LB liquid medium (100 mg/L of ampicillin, 160rpm at 37°C). The following day 200mL of LB liquid medium were inoculated with overnight preculture to an OD₆₀₀ of 0.1 and grown until optical density reached a value between 0.6 and 0.8 (160rpm, 37°C). Then cultures were induced with 0.5 mM IPTG and incubated for 16 h at 20 °C. Cells were collected and protein purification was performed as reported previously by De Vitis *et al.* through a gravimetric affinity chromatography with Nickel Affinity Gel (Sigma-Aldrich, USA). The purified protein (39.2 kDa) was dialyzed overnight against 50mM NaCl 100mM buffer at variable pH values (pH: 6.0, 7.0, 8.0, 8.5, 9.0), then protein purity was checked by SDS-PAGE (Figure S1 in Supplementary Material).

The isoelectric point of the His-tagged protein is $pH(I) = 5.72$. The $pH(I)$ value was calculated by the ExPASy-ProtParam tool.

Further details concerning the materials used are reported in the Supplementary Material (Table S1-4).

Enzymatic activity

Dialyzed proteins were concentrated with 10 kDa Vivaspin filters (Vivaspin 100 kDa; Sartorius, Göttingen, Germany) and enzymatic activity was checked spectrophotometrically at 400nm (15 000 M⁻¹ cm⁻¹) employing a protein concentration of about $1.5 \cdot 10^{-5}$ M in the presence of 0.015 mM p-

nitrophenyl acetate (pNPA) as substrate in different buffers (50 mM citrate buffer for pH 6.0; 50 mM TRIS-HCl buffer for pH 8.0, pH 8.5 and pH 9.0). An enzymatic activity unit of BCE corresponds to the amount of protein that produces 1 μ mol of p-nitrophenol, hydrolyzed form p-nitrophenyl acetate in one minute. Enzymatic assays at different temperature were performed preheating at the desired temperature buffers, protein and substrate for 15 min in a water bath while enzymatic assays were performed in a thermo-controlled spectrophotometer (Eppendorf, Germany). All samples were analyzed in triplicate and the experimental errors varied between 1% and 5%.

Differential Scanning Calorimetry

Calorimetric measurements were carried out on solutions with a protein concentration of about $1.5 \cdot 10^{-5}$ M in different buffers (50 mM citrate buffer + 100 mM NaCl for pH 6.0; 50 mM phosphate buffer + 100 mM NaCl for pH 7.0; 50 mM TRIS-HCl buffer + 100 mM NaCl for pH 8.0, pH 8.5 and pH 9.0) with a TA Instruments Nano-DSC 6300 (TA Instruments, USA) equipped with capillary cells. The calibration of the instrument was performed by the manufacturing service personnel by means of calibration pulses (Joule effect, instrument internal auto test). Measurements were carried out at $0.5^{\circ}\text{C} \cdot \text{min}^{-1}$ scanning rate, in the temperature range from 10°C to 95°C . Parallel measurements were also performed on solutions with a protein concentration of about $6 \cdot 10^{-5}$ M by using a Micro-DSCIII apparatus (Setaram, France), equipped with 1 mL hermetically closed cylindrical pans, at the same scanning rate. For this instrument, the calibration was performed by the manufacturing service personnel and tested by using the Joule effect calibrator EJ2 (Setaram, France). For all experiments, a heating-cooling cycle was scheduled, then followed by a second heating scan. With both equipment, the second heating scan produce flat traces (not reported). We would like to underline here, that the second heating scan is not an index to assess reversibility of the protein denaturation since the protein experiences the stress of high temperatures (*i.e.*, far from the denaturation temperature range) during the first heating (up to 95°C in our case) [20]. Indeed, the only reason we performed the second heating scan was to obtain a comparison for the baseline obtained from the buffer blank system.

Data were analyzed by means of the software THESEUS [23] following procedures reported in previous studies [20,24]. Briefly, the apparent molar heat capacity $C_P^{app}(T)$ of the sample was scaled with respect to a baseline across the scanned temperature range to obtain the excess molar heat capacity $C_P^{exc}(T)$ with respect the "native state", $C_{P,N}(T)$ (*i.e.*, the trend emerged from the pre-denaturation region). The denaturation specific heat drop, $\Delta_d C_P$, *i.e.*, the difference between the intrinsic denatured and native states' specific heats, was affected by a rather large error and was therefore not considered in the present work, with the exception of those runs at pH 8.5. Accordingly, a sigmoidal trend across the denaturation region was applied to scale the thermogram and eliminate

the $\Delta_d C_P$ drop contribution (see Supplementary material). All the thermograms reported in this article were scaled accordingly. The area underlying the recorded peaks, so treated and presented in the figures, directly corresponds to the relevant denaturation enthalpy, $\Delta_d H^\circ$, in $\text{kJ}\cdot\text{mol}^{-1}$ units. Errors were evaluated on the basis of at least three replicates. The fit attempts based on the denaturation thermodynamic models were accomplished using the nonlinear Levenberg–Marquardt method [25]. The error of each fitting parameter was calculated with a 95.4% confidence limit by the Monte Carlo simulation method and resulted to be lower than the experimental error. The temperatures that reflect the onset of the denaturation peaks were obtained from the thermodynamic fits by extrapolating the temperature values corresponding to the 1% height of the lowest profile (pH 9).

Results and discussion

Influence of pH on BCE thermal stability

It is well known that the stability of globular proteins, and in turn the range of their functionality, generally depends on the aqueous environment basing on the possible specific and/or not specific interactions that may establish [26–28], and one of the most relevant factors is the pH of the solution [29]. Aiming at characterizing the thermal stability of BCE in different process conditions, DSC measurements were performed at several pH values (pH 6.0, 7.0, 8.0, 8.5 and 9.0).

The results obtained using the micro-DSC instrument, which is equipped with normal cylindrical cells, were affected by severe aggregation effects that were observed almost in all cases. As an example, Figure 2 reports the thermograms obtained through micro-DSC for BCE at pH 8.0 and pH 8.5 (red and the green curves, respectively). As concerns the behaviour of BCE at pH 8.5, we observe a complex signal which consists of an endothermic peak reflecting the protein denaturation phenomenon followed by an exothermic peak due to the protein aggregation, whose onset is far enough to leave the denaturation peak practically unaffected by the delayed aggregation phenomena. By contrast, when the BCE sample is prepared at pH 8.0, the exothermic and the endothermic contributions are less spaced than the previous trace and aggregation clearly affects the denaturation trace. This tendency becomes progressively worse in the case of lower pH values where the aggregation phenomena become almost concomitant, and the protein provides micro-DSC thermograms that are characterised by an endothermic peak overlapped by a strong exothermic contribution ending with a noisy trace (Figure S2 in the Supplementary Material). At pH 6.0, the micro-DSC only recorded a very noisy trace with no visible unfolding peak.

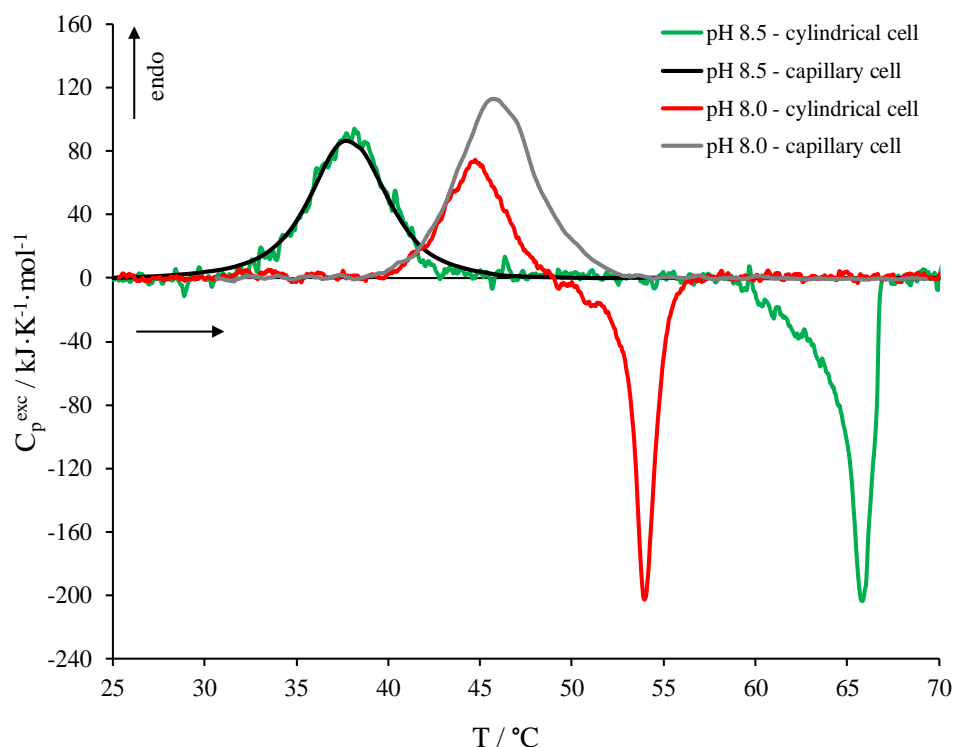


Figure 2. Thermograms obtained for BCE solutions in 50 mM TRIS-HCl buffer + 100 mM NaCl at pH 8.0 and pH 8.5 by using both a micro-DSC with cylindrical cell (red and green curves for pH 8.0 and pH 8.5, respectively) and a nano-DSC with capillary cells (grey and black curves for pH 8.0 and pH 8.5, respectively).

In order to avoid, or at least mitigate, the disturbance of the aggregation phenomena on the calorimetric profiles, measurements were also performed for all systems through a nano-DSC equipped with capillary cells. Indeed, literature reports that the capillary design often delays the aggregation kinetics [20]. The thermograms so obtained for BCE samples at pH 8.0 and pH 8.5 are reported in Figure 2 as grey and black traces, respectively. Both the calorimetric profiles exhibit a single endothermic peak, without any visible exothermic contribution.

The overall experimental traces obtained through the nano-DSC instrument for BCE thermal unfolding process are reported as circles profiles in Figure 3 with the exception of the trace obtained for pH 6 (full traces are also reported in Figure S3 in the Supplementary Material, including the trace for pH 6 – see below) and the overall corresponding thermodynamic parameters are reported in Table 1. We observe that the increase of the solution pH value reduces the protein thermal stability both in terms of enthalpic and entropic contributions (thermograms are shifted towards lower temperatures). The destabilization trend observed by increasing the pH of the solution with respect to the protein isoelectric point ($pH(I) = 5.72$ for BCE – see Materials and Methods) is in line with the models and theories applied for the quantification and interpretation of the pH dependence of protein stability in

1 terms of non-specific interactions, which account for a destabilizing effect as the net charge of the
2 protein increases [30]. In the same context, also the aggregation behaviour observed from the micro-
3 DSC traces in Figure 2 and Figure S2 can be correlated to the presence of increasingly higher negative
4 charges, whose electrostatic repulsion limits and delays the aggregation effects observed as the pH
5 increases [26].

6 However, beyond the general theoretical frame, each protein has a peculiar structure (*e.g.*, buried
7 ionisable groups [31], *etc.*) that has to be considered in details to attempt a quantitative theoretic
8 evaluation of the pH influence on the thermodynamic stability of this enzyme. Such an in depth
9 theoretical analysis is beyond the scope of this paper and we limit here to exploit the experimental
10 picture emerged.

11 12 13 Thermodynamic analysis

14 In order to assess whether the application of nano-DSC prevented the aggregation disturbances
15 allowing the characterization and quantification of the thermodynamic stability of the protein, various
16 thermodynamic models [32,33] were applied attempting the best fit of the theoretical curves to the
17 experimental data.

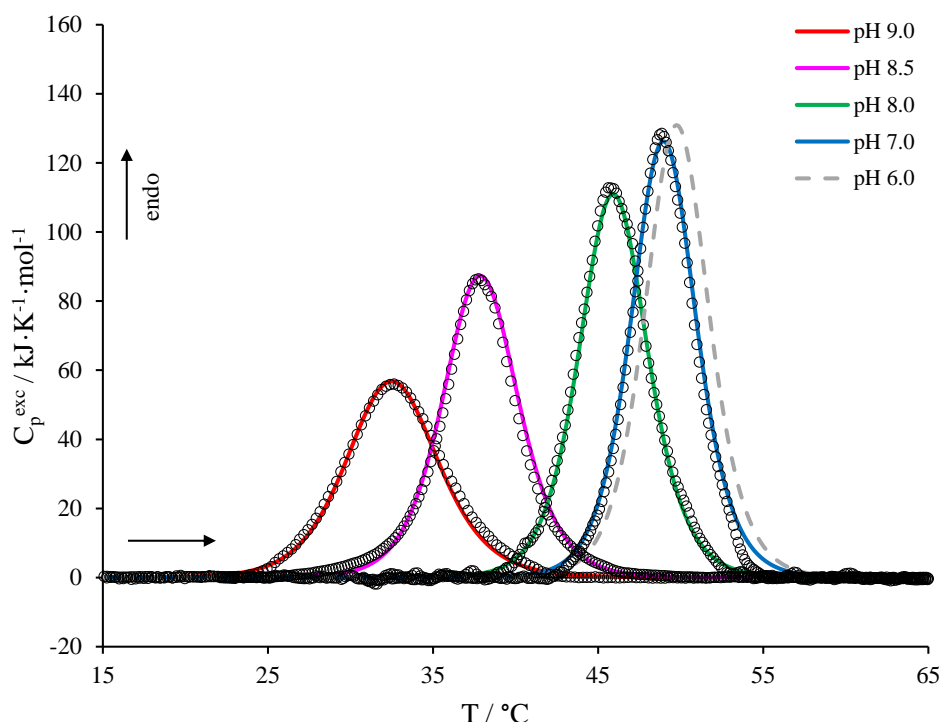


Figure 3. Nano-DSC thermograms from the first heating scan for BCE solutions at pH 7.0, pH 8.0, pH 8.5 and pH 9.0 (circles curves from right to left, respectively). The blue, green, magenta and red solid lines are the respective theoretical curves calculated according to a single-step denaturation model, whereas the dashed grey trace is the theoretical simulation attempted for BCE solutions at pH 6.0 by considering the data extrapolated from Figure 4.

Table 1: Protein denaturation enthalpy, $\Delta_d H^\circ$, and temperature, T_d , obtained both experimentally and by the best-fit of the DSC traces for BCE at different pH values, together with the temperature of the denaturation onset obtained as reported in the Materials and Methods section. Data were obtained at a protein concentration of about $1.5 \cdot 10^{-5}$ M in different buffers (50 mM citrate buffer + 100 mM NaCl for pH 6.0; 50 mM phosphate buffer + 100 mM NaCl for pH 7.0; 50 mM TRIS-HCl buffer + 100 mM NaCl for pH 8.0, pH 8.5 and pH 9.0). The fit parameters were calculated according to a one-step denaturation model.

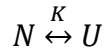
	Experimental values		One-step denaturation model Best-Fit parameters		
	$\Delta_d H^\circ / \text{kJ} \cdot \text{mol}^{-1}$	$T_d / ^\circ\text{C}$	$\Delta_d H^\circ / \text{kJ} \cdot \text{mol}^{-1}$	$T_d / ^\circ\text{C}$	$T_{\text{onset}} / ^\circ\text{C}$
pH 6.0	275 *	49.8	670 **	49.8	41.0
pH 7.0	615	48.9	660	49.0	40.2
pH 8.0	620	45.6	610	45.9	36.8
pH 8.5	515	37.7	530	37.9	28.2
pH 9.0	430	32.6	420	32.5	21.6

The errors for the experimental data are $\pm 5\%$ and $\pm 0.5^\circ\text{C}$ for $\Delta_d H^\circ$ and T_d , respectively. The uncertainties for the best-fit parameters (95.4% confidence limit) are lower than the experimental errors.

* apparent value because of severe aggregation phenomena

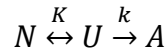
** the parameter for this pH was theoretically extrapolated from Kirchhoff's equation by considering the T_d revealed through the nano-DSC measurements. See also Figure 4.

The results obtained for the systems at pH 7.0, 8.0, 8.5 and 9.0 values showed that a single-step native-to-denatured state equilibrium model,



is sufficient to obtain a good fit for all the BCE solutions. The corresponding fitting curves are shown in Figure 3 (solid lines), whilst the respective best-fit thermodynamic parameters are reported in Table 1. The good fitting obtained with the simplest thermodynamic model that contemplate only two fitting parameters, *i.e.*, T_d and $\Delta_d H^\circ$, assures that the capillary design of the nano-DSC well limited the aggregation effects for these systems, allowing a deeper equilibrium thermodynamic exploitation of these data.

By contrast, the experimental enthalpy value obtained from the calorimetric trace of BCE at pH 6.0 (Figure S3 in the Supplementary Material) resulted very low and no equilibrium thermodynamic model produced a satisfactory fit though there is no reason for presuming that the denaturation mechanism has changed. Even the attempt of inclusion of a kinetic step in the above-mentioned model,



with a first order kinetic constant that aims at simulating the aggregation phenomena [32,34], did not produce any satisfactory fit. In any case, such specific details on the aggregation mechanism, which are also strictly dependent on the DSC cells geometry, is beyond the scope of this paper. Hence, we may conclude that, at pH 6.0, the aggregation phenomenon is so prominent that even the capillary cell calorimeter was not able to mitigate it sufficiently to allow a fair thermodynamic analysis in this case. Accordingly, we limited further thermodynamic considerations only to the systems at pH 7.0, 8.0, 8.5 and 9.0.

In order to get an estimation of the standard Gibbs energy of denaturation, $\Delta_d G^\circ(T)$, which basically dictates the protein thermodynamic stability and in turn the protein functionality [20] at each working temperature, the specific heat difference between the protein denatured and native states, $\Delta_d C_P$, needs to be known. In theory, this quantity may be directly obtained from the thermograms, but it is often affected by large errors due to baseline uncertainties. Specifically concerning our case, the direct measurement of the $\Delta_d C_P$ value was only feasible at pH 8.5 (Figure S4 in the Supplementary Material) and, being aware of the possible mistakes due to the signals' noise, we observed a $\Delta_d C_P \approx 14 \text{ kJ}\cdot\text{mol}^{-1}\cdot\text{K}^{-1}$.

In alternative, the $\Delta_d C_P$ value can be estimated by means of the Kirchhoff equation [23,29]

$$\Delta_d H^\circ(T) = \Delta_d H^\circ(T_d) + \Delta_d C_P \cdot (T - T_d) \quad (1)$$

obtained by assuming a constant $\Delta_d C_P$ value.

Figure 4 shows the $\Delta_d H^\circ$ -vs- T_d plot obtained by using the parameters from the one-step equilibrium denaturation model reported in Table 1.

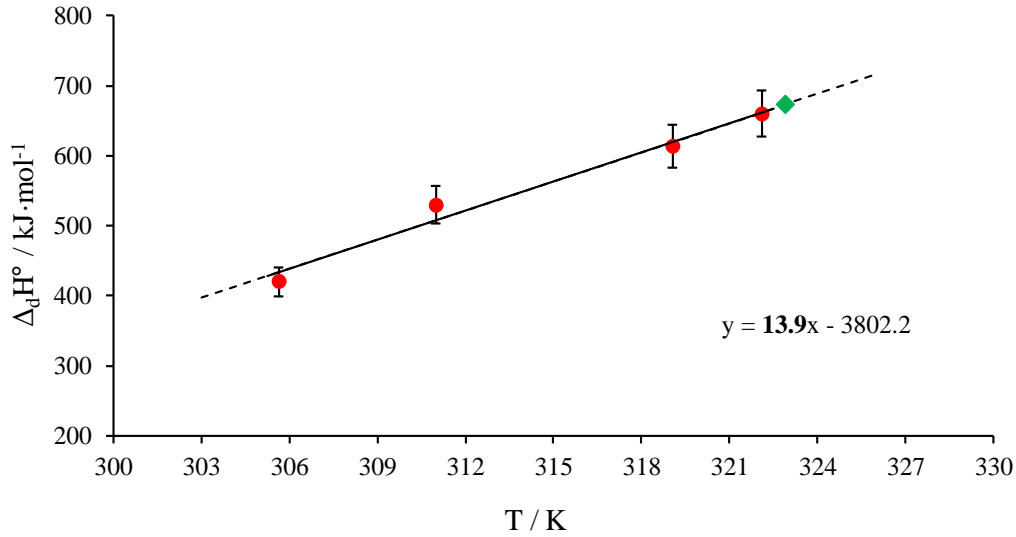


Figure 4. Plot of the protein denaturation enthalpy, $\Delta_d H^\circ$, versus the denaturation temperature, T_d , obtained for BCE at various pH values. The red dots represent the thermodynamic parameters for BCE solutions from pH 9.0 to pH 7.0 (already reported in Table 1), whilst the green square represents the theoretical extrapolation for pH 6.0 obtained by considering the T_d revealed through the nano-DSC measurements. The slope of the linear best-fit, whose equation is reported within the graph area in bold, represents the protein $\Delta_d C_P$ according to eq. 1.

We observe a linear trend that indicates that equation (1) is consistent with the experimental data, *i.e.*, in our system, the $\Delta_d C_P$ is practically independent from temperature. Accordingly, the slope of the linear best-fit corresponds to the $\Delta_d C_P$ value and resulted to be equal to $(14 \pm 2) \text{ kJ} \cdot \text{mol}^{-1} \cdot \text{K}^{-1}$. This value is coherent with those directly obtained from the thermograms at pH 8.5, where the reproducibility was acceptable (Figure S4 in the Supplementary Material). Furthermore, Figure 4 also reports an extrapolation of a theoretical $\Delta_d H^\circ$ for BCE at pH 6.0 carried out by using the apparent T_d (the peak maximum) obtained from the nano-DSC thermogram (grey curve in Figure S4), being aware that the T_d value might have been affected by the aggregation phenomena. The corresponding expected calorimetric profile was also simulated (theoretical C_P curve at pH 6) according to the previous one-step thermodynamic model for the sake of completeness (Table 1 and dashed grey profile in Figure 3).

The $\Delta_d C_P$ value and both the T_d and $\Delta_d H^\circ$ parameters obtained so far according to the one-step denaturation equilibrium model were used to calculate the $\Delta_d G^\circ(T)$ function

$$\Delta_d G^\circ(T) = \Delta_d H^\circ(T) - T_d \cdot \Delta_d S^\circ(T) \quad (2)$$

where $\Delta_d H^\circ(T)$ is given by equation (1) and $\Delta_d S^\circ(T)$ is given by the Kirchhoff's equation (3) [23,29]

$$\Delta_d S^\circ(T) = \Delta_d S^\circ(T_d) + \Delta_d C_P \cdot \ln(T/T_d) \quad (3)$$

Accordingly, the $\Delta_d G^\circ(T)$ function was obtained for BCE at each pH condition here considered, and the respective curves are reported in Figure 5. We observe that the $\Delta_d G^\circ(T)$ function presents a maximum, as expected [20,35,36], and becomes null at $T = T_d$ by definition. In the case of BCE, we observe that the overall $\Delta_d G^\circ(T)$ curves are progressively located at higher values as the pH decreases. For instance, if we consider $T = 25^\circ\text{C}$ as working temperature for a process involving the enzymatic activity of BCE, we observe the $\Delta_d G^\circ(25^\circ\text{C})$ values are different for each pH with increasing values as the pH decreases (values following the solid vertical line in Figure 5).

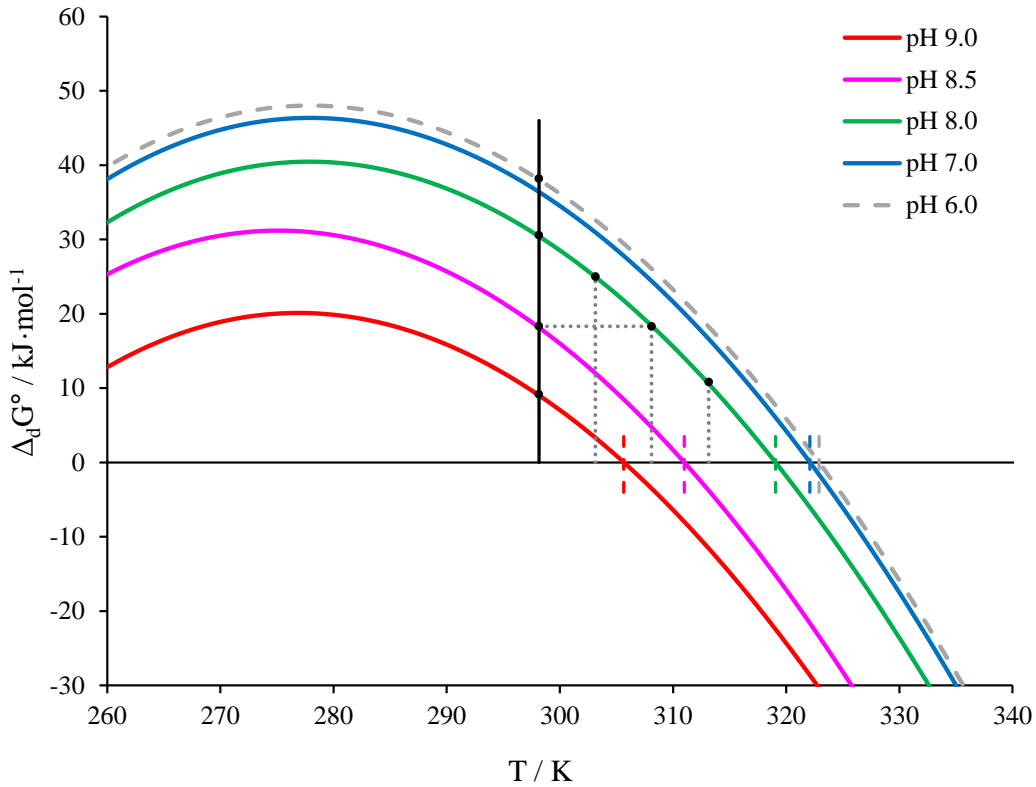


Figure 5. Estimation of the $\Delta_d G^\circ(T)$ trends for BCE at pH 7.0 (blue curve), pH 8.0 (green curve), pH 8.5 (magenta curve), pH 9.0 (red curve) and an attempt for BCE at pH 6.0 according to both the data reported in Table 1 and the $\Delta_d C_P$ provided by Figure 4. The respective vertical dashed lines indicate the corresponding denaturation temperatures T_d . For the sake of a better visualization, the black vertical line indicates $T = 25^\circ\text{C}$, whereas the black dots indicate the protein conditions (T and pH) for which specific activity measurements were performed.

Table 2: Specific activity data obtained for BCE (about $1.5 \cdot 10^{-5}$ M) at constant temperature ($T = 25^\circ\text{C}$) and in buffers at different pH values (50 mM citrate buffer for pH 6.0; 50 mM TRIS-HCl buffer for pH 8.0, pH 8.5 and pH 9.0; all buffers contained 0.015 mM p-nitrophenyl acetate (pNPA) as substrate).

Specific activity / $\text{U} \cdot \text{mg}^{-1}$	
pH 6.0	0.110 ± 0.009
pH 8.0	0.262 ± 0.018
pH 8.5	0.168 ± 0.020
pH 9.0	0.147 ± 0.007
The experimental errors are based on three replicates.	

Table 3: Specific activity data obtained for BCE (about $1.5 \cdot 10^{-5}$ M) at constant pH value (pH = 8.0, 50mM TRIS-HCl buffer in the presence of 0.015 mM p-nitrophenyl acetate (pNPA) as substrate) and at different temperatures.

Specific activity / $\text{U} \cdot \text{mg}^{-1}$	
$T = 25^\circ\text{C}$	0.262 ± 0.018
$T = 30^\circ\text{C}$	0.295 ± 0.130
$T = 35^\circ\text{C}$	0.450 ± 0.021
$T = 40^\circ\text{C}$	0.588 ± 0.059
The experimental errors are based on three replicates.	

In general, the optimal functionality of a protein, that is often expressed in physiological conditions, corresponds to a $\Delta_d G^\circ$ value between the $\Delta_d G^\circ(T_d)$, which is zero, and the maximum one. Indeed, such an energetic condition is a stability compromise that permits to obtain a protein resilient to the necessary energetic fluctuations (“protein flexibility”) that enable the protein function [37].

Accordingly, to assess the correlation between the protein stability in terms of $\Delta_d G^\circ$ and protein functionality, specific activity measurements were performed for BCE at $T = 25^\circ\text{C}$ and at the various pH values under investigation (Table 2). We observe a maximum specific activity at pH 8.0 that gives an indication of the optimal $\Delta_d G^\circ$ value ($\Delta_d G^\circ_{\text{opt}}$) at such a temperature. However, for this specific protein, we observed a good protein functionality among all the pH range considered and thus over a wide range of $\Delta_d G^\circ$ values. This result indicates that the specific structure of the protein is resilient to environmental changes as regards the enzymatic site functionality, offering additional possibilities in the research of the optimum working conditions.

1 In any case, for the assessment of the optimal working condition for an enzyme, we should in
2 general consider that the overall enzymatic activity is not only dictated by the protein
3 thermodynamics (optimal $\Delta_d G^\circ$) but also by kinetic factors, which are temperature dependent as well.

4 In this context, in order to assess whether the temperature-dependent kinetic effects prevail over
5 the pH-dependent thermodynamic effects on the protein functionality, further specific activity
6 measurements were accomplished. In particular, we selected the pH value corresponding to the
7 highest enzymatic specific activity at $T = 25^\circ\text{C}$ (*i.e.*, pH = 8.0, as reported in Table 2) and performed
8 measurements at higher temperatures, namely 30°C , 35°C and 40°C . The results show that the activity
9 increases with increasing temperature (Table 3) indicating that the kinetic benefits overwhelm the
10 thermodynamic disadvantage.

11 In any case, it is important to underline that the working temperature should always be kept well
12 below the onset of the denaturation process (Table 1) that also trigger the aggregation effects, the last
13 of which would lead to a continuous and irreversible loss of active enzyme. Indeed, the onset of the
14 denaturation process represents the condition at which the presence of the denatured protein fraction
15 starts to be statistically significant, and if the denaturation equilibrium is followed by a high-rate
16 aggregation, this kinetic step progressively displaces the denatured protein from the equilibrium,
17 resulting in a totally aggregated protein over time even if at constant T_w . In this regard, high starting
18 apparent values for the protein activity might be misleading and longer time for the process evolution
19 might be needed. However, such details are beyond the scope of this paper that is merely devoted to
20 draw the overall thermodynamic behavior of the BCE, which could be useful for an experimental
21 design that aims at maximizing the process efficiency.

22 We would like to emphasize that, in general, it is well known that the higher the working
23 temperature T_w chosen for a catalyst, the higher the rate of the process, as described by Arrhenius
24 equation. However, such a statement is valid only if no alterations affect the catalyst structure. For
25 example, the pure kinetic effect at the same thermodynamic condition, *i.e.*, same $\Delta_d G^\circ$, can be
26 recognised by comparing the specific activity values for BCE at pH 8.5 / $T = 25^\circ\text{C}$ and at pH 8.0 / T
27 $= 35^\circ\text{C}$ (Figure 5), which correspond to $0.168 \text{ U}\cdot\text{mg}^{-1}$ and $0.450 \text{ U}\cdot\text{mg}^{-1}$, respectively.

28 On the other hand, the fact that the kinetic benefits overwhelm the thermodynamic disadvantage
29 in a wide range of $\Delta_d G^\circ$ values is not a general condition but a specific characteristic of BCE revealed
30 by this study. However, we would like to underline here that the specific activity measurements were
31 performed using a model substrate. BCE efficiency on other substrates at different temperatures and
32 pH conditions needs to be singularly assessed in view of an industrial process design. Nonetheless
33 the methodological approach here applied has a general validity and may be useful as a guideline to
34 design enzyme optimal working conditions through calorimetric methods.

Conclusions

The calorimetric investigation presented in this study allowed the achievement of a detailed picture about the thermal stability and functionality of the carboxylesterase from *Bacillus coagulans* (BCE) over the pH range from 6 to 9.

Measurements accomplished through the calorimeter equipped with cylindrical cells revealed that protein thermal denaturation is followed by aggregation phenomena with downshifted onset as the pH of the environment decreases.

The use of the capillary cell calorimeter, aimed at avoiding/mitigating the aggregation disturbances, allowed the thermodynamic analysis of the system. We observed a protein thermal denaturation well in line with a single-step native-to-denatured state equilibrium mechanism for all the pH range investigated. The protein thermal stability decreases with increasing pH values in terms of both denaturation temperature and enthalpy. The application of Kirchhoff equation to the thermodynamic data indicated a temperature-independent $\Delta_d C_P$ value, permitting to obtain an estimation of the $\Delta_d G^\circ(T)$ trends for BCE at different pH values.

Specific activity measurements at 25°C permitted the correlation of BCE enzymatic activity with the $\Delta_d G^\circ(25^\circ\text{C}, \text{pH})$ calculated values. The results indicate that the maximum activity corresponds to the value of $\Delta_d G^\circ(25^\circ\text{C}, \text{pH } 8.0)$ but still a good enzymatic functionality is preserved in a wide range of $\Delta_d G^\circ$ values around the optimum. This peculiarity was exploited by performing specific activity measurements at higher temperatures (30°C, 35°C, 40°C) and the results indicated that the kinetic benefits at higher temperatures overwhelm the thermodynamic disadvantage. Accordingly, the optimal choice for the industrial application of BCE involves a solution at pH 8 if possible. In any case, the temperature parameter can be set up at the highest values admitted by the denaturation onset limit (Table 1) to avoid aggregation worries. However, we would like to underline here that more specific information related to each application can be achieved by associating the thermodynamic analysis here presented with the activity values for BCE in the presence of the desired substrate.

In conclusion, the thermodynamic analysis in combination with specific activity measurements is able to provide the necessary information for the assessment of BCE optimal working conditions.

Although the results here reported are restricted to the specific enzyme and model substrate used, the methodological approach and the thermodynamic exploitation here applied have a general validity and may be useful as guidelines to design enzyme optimal working conditions through calorimetric methods.

References

- [1] X. Fan, X. Niehus, G. Sandoval, Lipases and proteases, 2012.
- [2] P. Fojan, P.H. Jonson, M.T.N. Petersen, S.B. Petersen, What distinguishes an esterase from a lipase: A novel structural approach, *Biochimie*. 82 (2000) 1033–1041. doi:10.1016/S0300-9084(00)01188-3.
- [3] Y. Ben Ali, R. Verger, A. Abousalham, Lipases or Esterases: Does It Really Matter? Toward a New Bio-Physico-Chemical Classification, *Methods Mol. Biol.* 861 (2012) 31–51. doi:10.1007/978-1-61779-600-5_2.
- [4] Y. Jiang, K.L. Morley, J.D. Schrag, R.J. Kazlauskas, Different Active-Site Loop Orientation in Serine Hydrolases versus Acyltransferases, *ChemBioChem*. 12 (2011) 768–776. doi:10.1002/cbic.201000693.
- [5] U.T. Bornscheuer, Microbial carboxyl esterases: Classification, properties and application in biocatalysis, *FEMS Microbiol. Rev.* 26 (2002) 73–81. doi:10.1016/S0168-6445(01)00075-4.
- [6] Eijkmann C., Über Enzyme bei Bakterien und Schimmelpilzen, *Zentralbl Bakt Parasitenk Infekt.* 29 (1901) 841–848.
- [7] Uwe T. Bornscheuer and R. Joseph Kazlauskas, *Hydrolases in Organic Synthesis*, 2005. doi:10.1002/3527607668.
- [8] F. Hasan, A.A. Shah, A. Hameed, Industrial applications of microbial lipases, *Enzyme Microb. Technol.* 39 (2006) 235–251. doi:10.1016/j.enzmictec.2005.10.016.
- [9] S.H. Hamdan, J. Maingwa, M.S.M. Ali, Y.M. Normi, S. Sabri, T.C. Leow, Thermostable lipases and their dynamics of improved enzymatic properties, *Appl. Microbiol. Biotechnol.* 105 (2021) 7069–7094. doi:10.1007/s00253-021-11520-7.
- [10] U.U.M. Johan, R.N.Z.R.A. Rahman, N.H.A. Kamarudin, M.S.M. Ali, An integrated overview of bacterial carboxylesterase: Structure, function and biocatalytic applications, *Colloids Surfaces B Biointerfaces*. 205 (2021) 111882. doi:10.1016/j.colsurfb.2021.111882.
- [11] D. Romano, F. Bonomi, M.C. de Mattos, T. de Sousa Fonseca, M. da C.F. de Oliveira, F. Molinari, Esterases as stereoselective biocatalysts, *Biotechnol. Adv.* 33 (2015) 547–565. doi:10.1016/j.biotechadv.2015.01.006.
- [12] L. Steenkamp, D. Brady, Optimisation of stabilised Carboxylesterase NP for enantioselective hydrolysis of naproxen methyl ester, *Process Biochem.* 43 (2008) 1419–1426. doi:10.1016/j.procbio.2008.09.001.
- [13] M. Schmidt, E. Henke, B. Heinze, R. Kourist, A. Hidalgo, U.T. Bornscheuer, A versatile esterase from *Bacillus subtilis*: Cloning, expression characterization, and its application in biocatalysis, *Biotechnol. J.* 2 (2007) 249–253. doi:10.1002/biot.200600174.

- [14] V. Dachuri, C. Lee, S.H. Jang, Organic solvent-tolerant esterase from *sphingomonas glacialis* based on amino acid composition analysis: Cloning and characterization of EstSP2, J. Microbiol. Biotechnol. 28 (2018) 1502–1510. doi:10.4014/jmb.1806.06032.
- [15] Y.M. Mohamed, M.A. Ghazy, A. Sayed, A. Ouf, H. El-Dorry, R. Siam, Isolation and characterization of a heavy metal-resistant, thermophilic esterase from a Red Sea Brine Pool, Sci. Rep. 3 (2013) 1–8. doi:10.1038/srep03358.
- [16] X. Jiang, Y. Huo, H. Cheng, X. Zhang, X. Zhu, M. Wu, Cloning, expression and characterization of a halotolerant esterase from a marine bacterium *Pelagibacterium halotolerans* B2 T, Extremophiles. 16 (2012) 427–435. doi:10.1007/s00792-012-0442-3.
- [17] F. Molinari, O. Brenna, M. Valenti, F. Aragozzini, Isolation of a novel carboxylesterase from *Bacillus coagulans* with high enantioselectivity toward racemic esters of 1,2-O-isopropylideneglycerol, Enzyme Microb. Technol. 19 (1996) 551–556. doi:10.1016/S0141-0229(96)00066-X.
- [18] V. De Vitis, C. Nakhnoukh, A. Pinto, M.L. Contente, A. Barbiroli, M. Milani, M. Bolognesi, F. Molinari, L.J. Gourlay, D. Romano, A stereospecific carboxyl esterase from *Bacillus coagulans* hosting nonlipase activity within a lipase-like fold, FEBS J. 285 (2018) 903–914. doi:10.1111/febs.14368.
- [19] J. Jurczac, S. Pikul, T. Bauer, (R)- and (S)-2,3-O-isopropylideneglyceraldehyde in stereoselective organic synthesis, Tetrahedron Asymmetry. 42 (1986) 447–488.
- [20] C. Pelosi, F. Saitta, F.R. Wurm, D. Fessas, M.R. Tinè, C. Duce, Thermodynamic stability of myoglobin-poly(ethylene glycol) bioconjugates: A calorimetric study, Thermochim. Acta. 671 (2019) 26–31. doi:10.1016/j.tca.2018.11.001.
- [21] A. Cornish-Bowden, Principles of enzyme kinetics, Elsevier, 2014.
- [22] M.M. Stone, M.S. Weiss, C.L. Goodale, M.B. Adams, I.J. Fernandez, D.P. German, S.D. Allison, Temperature sensitivity of soil enzyme kinetics under N-fertilization in two temperate forests, Glob. Chang. Biol. 18 (2012) 1173–1184. doi:10.1111/j.1365-2486.2011.02545.x.
- [23] G. Barone, G., Del Vecchio, P., Fessas, D. Giancola, C., Graziano, Theseus: a new software package for the handling and analysis of thermal denaturation data of biological macromolecules, J. Therm. Anal. 39 (1993) 2779–2790.
- [24] M.H. Sleiman, R. Csonka, C. Arbez-Gindre, G.A. Heropoulos, T. Calogeropoulou, M. Signorelli, A. Schiraldi, B.R. Steele, D. Fessas, M. Micha-Screttas, Binding and stabilisation effects of glycodendritic compounds with peanut agglutinin, Int. J. Biol. Macromol. 80 (2015) 692–701. doi:10.1016/j.ijbiomac.2015.07.036.

- 1 [25] W.H. Press, B.P. Flannery, S.A. Teukolski, W.T. Weterling, Numerical recipes, Cambridge
2 Univ. Press Cambridge, UK. (1989) 289–293.
- 3 [26] L. Caldinelli, S. Iametti, A. Barbiroli, D. Fessas, F. Bonomi, L. Piubelli, G. Molla, L.
4 Pollegioni, Relevance of the flavin binding to the stability and folding of engineered
5 cholesterol oxidase containing noncovalently bound FAD, *Protein Sci.* 17 (2008) 409–419.
6 doi:10.1110/PS.073137708.
- 7 [27] A. Barbiroli, M. Marengo, D. Fessas, E. Ragg, S. Renzetti, F. Bonomi, S. Iametti,
8 Stabilization of beta-lactoglobulin by polyols and sugars against temperature-induced
9 denaturation involves diverse and specific structural regions of the protein, *Food Chem.* 234
10 (2017) 155–162. doi:10.1016/J.FOODCHEM.2017.04.132.
- 11 [28] C. Pelosi, F. Saitta, C. Zerino, G. Canil, T. Biver, A. Pratesi, C. Duce, D. Fessas, C.
12 Gabbiani, M.R. Tiné, Thermodynamic Evaluation of the Interactions between Anticancer
13 Pt(II) Complexes and Model Proteins, *Mol.* 2021, Vol. 26, Page 2376. 26 (2021) 2376.
14 doi:10.3390/MOLECULES26082376.
- 15 [29] P.L. Privalov, A.I. Dragan, Microcalorimetry of biological macromolecules, *Biophys. Chem.*
16 126 (2007) 16–24. doi:10.1016/J.BPC.2006.05.004.
- 17 [30] K.U. Linderstrøm-Lang, On the ionization of proteins, *CcCR Trav. Lab. Carlsb.* 15 (1924) 1–
18 29.
- 19 [31] D. Stigter, K.A. Dill, Charge effects on folded and unfolded proteins, *Biochemistry.* 29
20 (1990) 1262–1271. doi:10.1021/bi00457a023.
- 21 [32] A. Barbiroli, F. Bonomi, P. Ferranti, D. Fessas, A. Nasi, P. Rasmussen, S. Iametti, Bound
22 Fatty Acids Modulate the Sensitivity of Bovine β -Lactoglobulin to Chemical and Physical
23 Denaturation, *J. Agric. Food Chem.* 59 (2011) 5729–5737. doi:10.1021/jf200463u.
- 24 [33] A. Ausili, A. Pennacchio, M. Staiano, J.D. Dattelbaum, D. Fessas, A. Schiraldi, S. D’Auria,
25 Amino acid transport in thermophiles: Characterization of an arginine-binding protein from
26 *Thermotoga maritima*. 3. Conformational dynamics and stability, *J. Photochem. Photobiol. B*
27 *Biol.* 118 (2013) 66–73. doi:10.1016/J.JPHOTOBIOB.2012.11.004.
- 28 [34] D. Fessas, S. Iametti, A. Schiraldi, F. Bonomi, Thermal unfolding of monomeric and dimeric
29 β -lactoglobulins, *Eur. J. Biochem.* 268 (2001) 5439–5448. doi:10.1046/j.0014-
30 2956.2001.02484.x.
- 31 [35] G.I. Makhatadze, P.L. Privalov, Energetics of protein structure., *Adv. Protein Chem.* 47
32 (1995) 307–425.
- 33 [36] W. Pfeil, P.L. Privalov, Thermodynamic investigations of proteins: III. Thermodynamic
34 description of lysozyme, *Biophys. Chem.* 4 (1976) 41–50.

1 [37] M. D'Onofrio, L. Ragona, D. Fessas, M. Signorelli, R. Ugolini, M. Pedò, M. Assfalg, H.
2 Molinari, NMR unfolding studies on a liver bile acid binding protein reveal a global two-
3 state unfolding and localized singular behaviors, Arch. Biochem. Biophys. 481 (2009) 21–
4 29. doi:10.1016/J.ABB.2008.10.017.
5
6
7
8